Dysfunctional dopaminergic neurones in mouse models of Huntington's disease

Glenn M Dallérac[a#], Grégoire Levasseur[b]*, Sarat C Vatsavayai[b]*, Austen J Milnerwood[a], Damian M Cummings[a], Igor Kraev[a], Chloé Huetz[b], Karen A Evans[a], Steve W Walters[a], Payam Rezaie[a], Yoon Cho[c], Mark C Hirst[a] and Kerry PSJ Murphy[a#].

a: *Huntington's Disease Research Forum, Department of Life, Health and Chemical Sciences, The Open University, Walton Hall, Milton Keynes, MK7 6AA, UK*.

b: *Centre de Neuroscience Université Paris Sud, CNRS UMR8195, Orsay, France.*

c: *Institut de Neurosciences cognitives et intégratives d'Aquitaine Université de Bordeaux 1, CNRS UMR 5287, Talence, France.*

[#].To whom correspondence should be addressed at: Department of Life, Health and Chemical Sciences, The Open University, Walton Hall, Milton Keynes, UK . Tel: +44(0)1908652917; Fax: +44(0)1908654167; Email: kerry.murphy@open.ac.uk, glenn.dallerac@college-de-france.fr.

* Equal contribution (co-second author)

Present addresses:

GMD: Centre Interdisciplinaire de Recherche en Biologie, CNRS UMR 7241/INSERM U1050, Collège de France, 11 place Marcelin Berthelot 75005 Paris, France.

SCV: Department of Neurology, University of California San Francisco, 675 Nelson Rising Lane, San Francisco CA 94158.

AJM: Brain Research Centre, University of British Columbia, Vancouver, Canada.

DMC: Department of Neuroscience, Physiology and Pharmacology, University College London, London, WC1E 6BT, U.K.

Keywords: dopamine, amperometry, SK3 channels, huntingtin, CAG expansion, *Substantia Nigra*, neurodegeneration, R6/1, polyglutamine.

Abstract

Background: Huntington's disease (HD) is a late-onset fatal neurodegenerative disorder caused by a CAG trinucleotide repeat expansion in the gene coding for the protein huntingtin, and is characterised by progressive motor, psychiatric and cognitive decline. We previously demonstrated that normal synaptic function in HD could be restored by application of dopamine receptor agonists, suggesting that changes in release or bioavailability of dopamine may be a contributing factor to the disease process.

Objective: In the present study, we examined the properties of midbrain DA neurones and dopamine release in presymptomatic and symptomatic transgenic HD mice.

Methods & Results: Using intracellular sharp recordings and immunohistochemistry we found that neuronal excitability was increased due to a loss of afterhyperpolarisation (sAHP) and that these changes were related to an apparent functional loss and abnormal distribution of SK3 ($K_{Ca}2.3$) channels, a class of small conductance calcium-activated potassium channels. Electrochemical detection of dopamine showed that this observation was associated with an enhanced dopamine release in presymptomatic transgenic mice and near extinction in symptomatic animals. These changes occurred in the context of a progressive expansion in CAG repeat number and nuclear localisation of mutant protein within the *Substantia Nigra pars compacta*.

Conclusions: Dopaminergic neuronal dysfunction is a key early event in HD disease progression. The initial increase in dopamine release appears to be related to a loss of SK3 channel function, a protein containing a polyglutamine tract. Implications for polyglutamine-mediated sequestration of SK3 channels, dopamine-associated DNA damage and CAG expansion are discussed in the context of HD.

Introduction

Huntington's disease (HD) is a fatal neurodegenerative disorder that belongs to the polyglutamine family of trinucleotide repeat diseases. For HD, a repeat CAG codon occurs within the first exon of the gene encoding the protein huntingtin [1] and the age of onset of this disorder is inversely correlated to the length of the CAG repeat expansion [2]. In humans, the symptoms which usually appear in the third to fifth decades of life often include cognitive disturbances that can over time develop into dementia [3]. The primary sites of neurodegeneration are the striatum and cerebral cortex [4–7] and neurological investigations suggest that early cognitive deficits may already be apparent in patients before the onset of classical symptoms [8–12]. Furthermore, post-mortem studies [7] reveal that both motor and cognitive symptoms can appear in the absence of overt neuronal cell loss, suggesting that impaired cognition is likely to be caused by synaptic and neural dysfunction rather than a consequence of cell death. With the introduction of genetic testing for the HD gene it is now possible to assess the cognitive performance of known gene carriers prior to the onset of overt motor symptoms. Importantly, such studies report that deficits in working memory, executive function [13,14] and certain aspects of recognition memory [15] are early events and occur prior to the onset of overt symptoms. These differences may reflect the variety of transgenic models studied.

The neurotransmitter dopamine is a powerful modulator of the synaptic plasticity believed to underlie these forms of cognition and dopaminergic (DA) deficits have been reported in presymptomatic and early-state symptomatic HD gene carriers. PET scanning studies have revealed that the density of functional D_1- and D_2- dopamine receptors are reduced in the striatum and cortex of these individuals [16–19], indicating that changes in the DA system are amongst the earliest detected in HD. However, the role of dopamine as a potential pathogenic agent in HD remains controversial [20,21] and human post mortem studies have yielded inconsistent results in terms of changes in brain dopamine levels.

The identification of the HD gene in 1993 [22] has led to the successful creation of several genetically modified mouse and rat models that recapitulate aspects of the human disease [reviewed in 23]. Studies using these genetic models have also added to the controversy, with some laboratories reporting dramatic reductions in striatal dopamine levels [24–27] or loss of dopamine signalling [28,29] and others suggesting that dopamine levels may be elevated [30] or toxic [31,32].

Surprisingly, very little is known about the properties of the HD midbrain DA neurones, the main source of dopamine in the brain. We report here a series of experiments designed to assess the properties of these neurones in terms of their (i) functional membrane characteristics, (ii) ability to release dopamine, (iii) expression of key proteins and (iv) CAG repeat expansion profile. We have used age-matched transgenic mice carrying 89 (R6/1-89Q line) and 116 CAG repeats (R6/1 line) corresponding to a prodomal and symptomatic state, respectively; an approach that has enabled us to characterize the nature of DA dysfunction in models of pre-manifest and manifest disease.

Material and Methods

Intracellular recording of DA neurones

Experiments were conducted in acute slices prepared from adult mice aged 7-10 months. At this age, R6/1-89Q mice are prodomal while R6/1 mice are close to the end-stage of the disease [33]. Coronal brain slices containing midbrain were prepared from transgenic and non-transgenic littermates, obtained from an in-house R6/1 mouse colony, maintained by breeding hemizygotic R6/1 and R6/1-89Q males with B6/CBA females housed in an enriched environment [34]. Briefly, mice were sacrificed by cervical dislocation and decapitation in accordance with UK legislation (Animal Scientific Procedures Act 1986). Measures were taken to minimize pain and discomfort. The brain was rapidly removed and placed in chilled (1-4°C) artificial cerebrospinal fluid (aCSF composition in mM: 120 NaCl, 4.7 KCl, 2.5 $CaCl_2$, 1.2 $MgSO_4$, 1.2 NaH2PO_4, 26 $NaHCO_3$, 11.5 D-Glucose). The cerebellum was removed and the brain glued at the caudal aspect to a silicone stage. Two 400 μm thick coronal section containing the *Substantia Nigra pars compacta* (*SNc*) and ventral tegmental area (VTA) (~ 3 mm posterior to bregma) were obtained from each mouse using a manual vibratome (Campden Instrument, Ltd, Sileby, UK). Slices were then transferred into an interface recording chamber (Scientific Systems Design Inc., Mercerville, NJ, U.S.A.) heated at 34°C (Proportional temperature Controller; ScientificSystems Design Inc.) and continuously perfused with oxygenated aCSF (95% O_2 and 5% CO_2, Carbogen, British Oxygen Company) at a flow rate of ~200 μl/min. Once placed in the recording chamber, slices were allowed to recover for >90 minutes prior to recording.

Intracellular recordings were obtained from neurones in the *SNc*/VTA with sharp electrodes (impedance 70-150MΩ) filled with 3M potassium acetate (KAc) and connected to an

Axoclamp2B DC amplifier (Axon Instruments Inc. USA) operated in bridge mode (current clamp). Electrical signals were visualised on an oscilloscope and digitized via an ITC-16 computer interface A/D converter (Instrutech Corp, NY, USA) coupled to a personal computer (MAC-G3, Apple Macintosh Inc. USA). Responses were collected and analysed using A/Dvance P3.61g software (Robert McKellar Douglas, Vancouver, CA).

Passive membrane properties were recorded by stepwise current injections (-1 to +1 nA, 500 ms) to generate a current–voltage (I/V) relationship, including positive pulses to assess action potential (AP) characteristics. Passive membrane properties were inferred from the I/V curve except membrane time constants (T_0), which were determined by analysing the time course of the membrane voltage deflection according to the method described by Rall [35,36]. This method consists in "peeling exponentials" by plotting the natural log of the response expressed as a percentage of the peak negative potential (Figure 1F). In our recordings, the late portion of the charging phase (for time points between 5 and 15 ms) always fitted a linear regression ($0.85<R^2<0.99$), of which the slope was equal to $-1/T_0$. For each cell and hyperpolarising intensity, the membrane time constant was thus calculated using this equation. Rall's method also allows determination of the equalizing time constant (T_1), which represents the time required for the current to spread to the proximal dendrites. T_1 is given by the second order exponential observed for time points earlier than 5 ms in Figure 1F. This value could thus be obtained by plotting the difference between the membrane time constant regression line from the points lying above this line, normalising the y-intercept of this new line ($0.77<R^2<0.99$) to 100% and reading T_1 as the negative inverse of the slope. From two time constants, the somatodendritic electronic length could be estimated using the relation: $L= \pi (T_0/T_1)^{-1/2}$.

Dopamine neurones were recognized by their characteristic electrical properties (Figure 1); that is, a long duration action potential with a typical hump on the downward slope (Figure 1D), a prominent time-dependent rectification, and a delayed repolarisation following cessation of an hyperpolarising current pulse (Figure 1C) [36–38].

Electrochemical detection of dopamine release

Slices were prepared from adult mice as above, with the exception that a single 400μm coronal section of the Caudate Putamen (CPu) was prepared (~0.5 mm anterior to bregma) from each animal. The slice was then transferred into an interface chamber and perfused with

heated (28°C), oxygenated aCSF at a flow rate of ~200 µl/min. Slices were left to equilibrate for >90min prior to recording.

For constant potential amperometry, +300 mV *vs* Ag/AgCl was applied to a carbon fibre electrode using the MicroC potentiostat (World Precision Instruments, Hertfordshire, UK). When present at the tip of the electrode, dopamine becomes oxidised, thereby generating a measurable faradaic current [39] that exhibits a linear relationship to dopamine concentrations ranging from 0.1 to 10 µM (Figure 4A). Recording carbon fibre electrodes (impedance 0.35-1.9 MΩ; CF30-100; World Precision Instruments, UK) were connected to a MicroC potentiostat (World Precision Instruments, UK) and the recorded signal sent to an ITC-16 computer interface A/D converter coupled to a Macintosh G3 personal computer. Responses were collected using A/Dvance P3.61g software which was also set to control Neurolog isolated stimulator boxes (NL800, Digitimer Ltd, UK). Calibration of the electrode was carried out for each experiment.

Stimulation of the striatal tissue was performed using stainless steel bipolar electrodes (World Precision Instruments, UK) placed in the dorsolateral striatum. The recording electrode was positioned approximately 500 µm ventral to the stimulating electrode, equidistant from the two the poles of the stimulating electrode. Input/output (I/O) relationships were obtained by incrementally stimulating the tissue once every 5 minutes (0.0033Hz, 40 µs, 20 - 500 µA). The stimulation strength giving the maximal amplitude was chosen as test shock for subsequent experiments. The maximum level of dopamine release (DA max) was obtained by averaging seven stimulations (35 min in total) at which dopamine release was maximal. Paired-pulse experiments consisted in applying two identical stimuli every five minutes with increasing inter-pulse intervals (ISI), from 50 ms to 50 s. Data were analysed for each interval by plotting the amplitude of the second response (P2) as a percentage of the first (P1) using the following formula: (P2/P1 x 100) -100.

SK3/TH/S830 Immunofluorescence

Triple immunodetection of tyrosine hydroxylase, mutant huntingtin and SK3 channels in the *SNc* was performed on 6 months old R6/1 animals (R6/1 n=5, non-transgenic littermates n=5), as well as presymptomatic 10 and symptomatic 20 months old R6/1-89Q mice (R6/1-89Q n=5, non-transgenic littermates n=5, for each age). Mice were perfused with 4% paraformaldehyde, pH 7.4. Brains were subsequently processed in 30 µm serial coronal sections by mean of a vibrating microtome (VT1000S; Leica, Milton Keynes,UK). For each

brain, 8 evenly spaced (180 µm) sections covering the total length of the *SNc* were taken starting from the principal mammillary tract and were processed for immunohistochemistry. After three successive rinses in 0.1M PBS, slices were transferred in a 0.5% BSA/0.2% Triton X-100/0.1M PBS (1X PBT) solution for 30 minutes and then incubated with constant agitation for 24h at 4°C in the primary antibodies cocktail (sheep anti-S830 polyclonal antibody (kind gift from Prof. Gillian Bates FRS) 1:5000, mouse anti-TH polyclonal antibody1:10000 (Abcam, UK) and rabbit polyclonal anti-SK3 (C-terminal) antibody 1:1000 (ab83737, Abcam, UK) diluted in 1X PBT, and rinsed three times in 0.1M PBS. Sections were then incubated with the secondary antibodies cocktail (Alexa-555 conjugated donkey anti-sheep, Alexa-488 goat anti-mouse and Alexa-633 goat anti-rabbit; 1:1000, Invitrogen) for 2 h at RT. After a last set of three rinses, sections were mounted using vectashield containing DAPI for confocal microscopy analysis (Zeiss LSM700 confocal microscope). Controls consisted in omitting the primary antibody for each target (except for tyrosine hydroxylase) and were performed independently.

All sections used for analysis were processed on the same day and with the same buffers and antibodies cocktails. All images were acquired using a 40X magnification lens and a numerical zoom set to 1X. Randomly chosen acquisition fields were taken from the *SNc* which was detected based on the TH signal. Image acquisition was done using a constant configuration for the SK3 signal detection (488 channel) across the whole set of sections. Quantification of fluorescence intensity was performed after acquisition of 3 acquisition fields (within the *SNc)* per slice (n=6 slices per animal). Masks for cell shapes, nuclear regions and HTT aggregates were designed independently for each image on specific channels (SK3/TH, DAPI and S830 respectively) using Adobe Photoshop. Fluorescence intensity of SK3 signals was quantified using these masks on the adequate channel image (green/488). This was performed using a custom Matlab (Matworks) scripts enabling categorization of regions of interests (ROI : nucleus *vs* cytoplasm, aggregate positive *vs* negative cells; TH *vs* non-TH cells) as well as quantification of the mean fluorescence intensity for each ROI.

Statistical analyses

Data for each condition were pooled and expressed as mean ± SEM. One- or two-way ANOVA were carried out as appropriate using Statistica 6.1 (StatSoft Inc.) or GraphPad Prism 5.00. Normal distribution of the datasets was verified using the Kolmogorov-Smirnov test and the Newman-Keuls test was used for post-hoc analyses. When datasets were found to

display a distribution significantly different from normal, the non-parametric Krustal-Wallis H-test was used. Differences between means for experimental and control conditions were considered statistically significant when $p<0.05$.

Somatic CAG repeat length analysis

CAG length analysis was performed on both mRNA and gDNA. For mRNA analysis, *SNc* was dissected from freshly sacrificed R6/1-89Q mouse and mRNA isolated using RNAspin reagents (GE Healthcare, UK) and a cDNA copy generated using cloned AMV reverse transciptase (Invitrogen, UK). cDNA synthesis was performed using a reaction mixture containing 5 μM of HD4 primer (5' GGCGGCTGAGGAAGCTGAGGA 3'), 10 mM dNTPs, cDNA synthesis buffer, 0.05 M DTT, 20 units of RNaseOUT and 7.5 units of cloned AMV RT. For each of the tissue sample, a negative control reaction was also prepared. Reactions were incubated for 50ºC (60 min), 85ºC (5 min) and stored at -20ºC.

CAG repeat length analysis was first performed on samples of cDNA that had been serially diluted in TE buffer containing 0.1 μM HD4 primer. Dilutions generating optimum amplification of discrete alleles were then used as templates for multiple independent PCR reactions, each containing 0.2 mM dNTPs, 0.5 μM of IR-800 labelled HD1 (5'ATGAAGGCCTTCGAGTCCCTCAAGTCCTTC 3') and HD4 (5' GGCGGCTGAGGAAGCTGAGGA 3') primers, 1X PCR buffer (Sigma, UK), 0.25% of DMSO and 1 unit *Taq* DNA polymerase (Sigma, UK). Reactions were heated to 94˚C for 2 min followed by 38 cycles of 94˚C for 30 s, 68˚C for 30 s and 72˚C for 2 min and followed by a final extension of 10 min at 72˚C in an Opticon 2 DNA Engine (M J Research Inc. U.S.A). Discrete alleles were resolved and visualised using 5% denaturing polyacrylamide electrophoresis on a Li-COR 4200 DNA sequencer. Individual alleles were sized against known size markers, their frequency scored and compared in a graph form to provide a visual representation of CAG expansion profile.

For gDNA analysis, DNA was first isolated from fresh *SNc* tissue samples after homogenisation, lysis and phenol-chloroform extraction [33] and stored at –20^{o}C until analysis. After quantitation at 260nm (Gene Quant Pro, Amersham Biosciences, UK), template DNA stocks were created by serial dilution in TE buffer containing 0.1 μM HD1 primer to a final concentration between 0.1-0.5 ng/μl. CAG alleles were amplified in reactions containing 0.2 mM dNTPs, 0.5 μM of each HD1 and IR800 labelled HD4 primers, 1X PCR buffer (Sigma, UK), 0.25% DMSO and 1 unit of *Taq* DNA polymerase (Sigma, UK).

Multiple independent PCR reactions were performed and resolution and detection were as described for cDNA analysis.

Results

Electrophysiological profile of DA neurones in transgenic mice

Passive membrane properties of transgenic DA cells (R6/1: n= 16, R6/1-89Q: n=17) were similar to those of non-transgenic DA neurones (n=48, Table 1 & Figure 2A). No significant genotype effect could be detected with respect to resting membrane potential, input resistance, membrane time constant, electronic length, and capacitance, thereby suggesting that the integrity of the membrane of transgenic DA neurones was not affected by the presence of either 89 or 116Q transgenic protein. Yet, spontaneous action potentials (AP) of R6/1 and R6/1-89Q DA neurones revealed a marked reduction of the slow afterhyperpolarisation (sAHP; Table 2 & Figure 2B-C; $p<0.001$). This impairment was more prominent in symptomatic R6/1 as compared to R6/1-89Q neurones ($p<0.001$) and resulted in an increased firing rate (Figure 2B; controls: 1.9± 0.2 Hz; R6/1-89Q: 3.9± 0.2 Hz; R6/1: 3.5± 0.2Hz; $p<0.05$).

The main function of the AHP is to regulate post-spike excitability. This, together with the slow oscillatory potential, regulates the spontaneous firing rate of DA neurones as well as neuronal excitability in response to depolarising inputs [36,40]. The latter phenomenon is termed accommodation and was assessed by injecting depolarising square current pulses of increasing intensities through the recording electrode. Non-transgenic DA neurones typically responded by a rapid accommodation of their firing rate; i.e. increasing inter-spike interval as the depolarisation persists (Figure 3A). In contrast, DA neurones firing upon depolarisation was severely impaired as shown by an increased instantaneous frequency (Figure 3B; controls: 76.1±7.1 Hz, R6/1-89Q: 103.7±9.4 Hz; R6/1: 116.4±10.3 Hz; $p<0.01$) and total frequency (Figure 3C; controls: 8.04±0.53 Hz, R6/1-89Q: 15.33±1.81 Hz; R6/1: 10.14±1.51 Hz, $p<0.001$). The ability of DA neurones to accommodate their firing rate upon excitation was more accurately assessed by calculating the percentage change between consecutive inter-spike intervals. Figure 3D shows that in non-transgenic DA neurones the maximal level of accommodation occurred at the beginning of the depolarising pulse. This initial accommodation was consistently impaired in transgenic cells (Figure 3D; $p<0.01$). Together, these data indicate that in HD DA neurones, sAHP dysfunction results in a markedly impaired

accommodation and as a consequence, drives the transgenic neurones into a hyper-excitable state.

Real-time measure of striatal dopamine release

We next reasoned that this hyper-excitability of DA neurones may translate in an increased release of dopamine at the synaptic terminals [41]. In order to test this hypothesis, we used constant potential amperometry in striatal slices to examine the evoked release of dopamine since the striatum is exquisitely vulnerable in HD and receives the highest density of DA input in the brain. Single electrical stimulations were sufficient to generate faradaic signals consisting of a brief stimulus artefact, a relatively rapid rise reaching its maximum at about 400-500 ms and a slow decay terminating at baseline approximately 2500-3000 ms following stimulation (Figure 4B). In order to confirm the faradaic nature of the signal, the electrode was regularly set to zero instead of +300 mV. Under such conditions, no response to electrical stimulation could be recorded, indicating that signals obtained at +300 mV were indeed due to redox reactions at the tip of the electrode.

Input/output relationships revealed that dopamine release was increased in R6/1-89Q mice (Figure 4C; DAmax values for non-transgenic slices: 2.9 ± 0.3 μM, n=6; R6/1-89Q: 4.2 ± 0.4 μM, n=8; $p<0.05$) while in slices prepared from R6/1 mice the release of striatal dopamine was drastically reduced (DAmax 0.8 ± 0.2 μM, n=5; $p<0.001$). We also assessed short-term plasticity of dopamine release by applying paired-pulse stimulation at different inter-stimuli intervals (ISI) and found no difference in prodomal R6/1-89Q mice as compared to control littermates, whereas R6/1 regulation of dopamine release was again severely compromised (Figure 4D, $p<0.001$). In all, these data suggest that enhanced dopamine release may underlie the early cognitive impairment reported in presymptomatic HD gene carriers, whilst the apparent loss of dopamine is entirely consistent with the hypokinetic state associated with end-stage HD [42].

SK3 immunostaining

The regulation of tonic firing in DA neurones is mediated by SK3 channels, a class of calcium sensitive small conductance potassium channels that generates the sAHP [43,44]. The SK3 channel carries a polyglutamine stretch close to its intracellular NH_2 terminus, and thus potentially constitutes a target for the expanded polyglutamine-containing transgenic protein,

which may prevent the insertion of SK3 channel subunits into the membrane during synthesis or disrupt channel function. In order to ascertain whether the expression of SK3 channels in DA neurones is influenced by polyglutamine-containing transgenic protein, we assessed the expression of both the SK3 channel protein and the transgenic protein in DA neurones (TH-positive) in the *SNc*. We first performed an immunocytochemical analysis using a triple α-SK3, α-tyrosine hydroxylase (TH), and α-S830 staining in the *SNc* of symptomatic R6/1 (n=5 mice) compared to their aged-matched non-transgenic littermates (n=5 mice). Interestingly, quantification of the SK3 levels in TH-positive cells (DA neurones) revealed a marked increase in R6/1 cells as compared to controls (Figure 5A, B; +41.40 ± 5.60%; $p<0.05$). Furthermore, this effect was significantly more prominent in TH-positive cells displaying cellular aggregates compared to TH-positive transgenic cells where no S830 staining could be detected (Figure 5A, $p<0.001$). We subsequently analyzed the intracellular distribution of SK3 staining and found that whilst SK3 staining is significantly higher in the cytosolic compartment of non-transgenic TH-positive cells (Figure 5A, D; $p<0.001$), the levels of SK3 are both elevated in the nucleus and cytosol of R6/1 TH-positive cells (Figure 5A, D, $p>0.05$; interaction genotype x compartment: $p<0.001$). This suggests that some of the SK3 channel proteins are translocated in the nucleus. Further, the redistribution of SK3 protein within transgenic TH-positive cells was found not to be dependent on the presence of frank nuclear S830-positive protein aggregates ($p>0.05$).

Interestingly, SK3 staining was found to be higher in TH-negative cells ($p<0.001$). However, quantification revealed no change in the amount of SK3 immunoreactivity in R6/1 non-DA cells when compared with non-transgenic ones (Figure 5C, -0.82 ± 2.41%; $p>0.05$). Taken together, these data suggest that the alterations in SK3 protein localization in R6/1 *SNc* are specific to DA neurones.

We then examined expression of the SK3 protein in R6/1-89Q animals before and after phenotype development by performing a similar immunocytochemical analysis, focusing on TH-positive cells in material prepared from 10 month old animals (prodomal R6/1-89Q, n=5; non-transgenic littermates, n=5) and 20 months old animals (symptomatic R6/1-89Q n=5; non-transgenic littermates, n=5). SK3 levels were found to be significantly increased in R6/1- 89Q TH-positive cells at both ages, indicating that this change in expression is an early event in disease progression (Figure 6, +38.30 ± 4.06%, $p<0.001$ at 10 months and + 14.20 ± 3.741 $p<0.05$ at 20 months of age) .

CAG repeat expansion in the SNc

The observation that the age of HD onset is inversely correlated with the repeat length implies that the deleterious consequences of the polyglutamine stretch are length dependent. Cells in the most severely affected brain regions in HD have been shown to undergo extensive repeat expansion long before disease onset [45–47] suggesting that somatic repeat expansion may be a cause or a consequence of cellular dysfunction. In order to assess whether CAG repeat expansion is a characteristic of DA neurones in HD and an early event in neuronal dysfunction, we assessed the extent of CAG repeat expansion in excised samples of *SNc* from R6/1-89Q mice at 2, 12 and 15 months of age.

Genomic DNA analysis revealed that somatic CAG repeat instability occurred as early as 2 months of age in the *SNc* (Figure 7A). Repeat instability comprised alleles with both expansions and truncations. At 12 months of age the instability observed was more pronounced and displayed a bias towards expansion. At 2 months old (2MO) the largest expansions observed in 1.89% of the alleles was 11 repeats, whereas 46.80 % at 12MO displayed an expansion >10 repeats with a maximum of 47 repeats. Overall, 66.04 % and 82.98% of cells located in the *SNc* displayed an increase in CAG repeat length at 2 and 12 months of age respectively (2MO mean expansion: 3.14±0.4 repeats, 12MO mean expansion: 16.56±2.21 repeats).

Since elongation of the CAG repeat in the genomic DNA may not be transcribed into mRNA, repeat instability analysis was also performed on cDNA products obtained from mRNA samples from the *SNc*. Akin to the gDNA data, the mRNA expansion profile revealed progressive elongations at every age studied (Figure 7B; 35.71 % of cells at 2MO with a mean expansion of 5.80±3.33 repeats and 77.34 % of cells at 15MO with a mean expansion of 17.28±1.18 repeats).

Altogether, our gDNA and cDNA CAG repeat analyses suggest that cells within the *SNc* expressing the transgene contain a protein with a progressively lengthening stretch of polyglutamine. This has the potential to interact with, and disrupt the function of other polyglutamine-containing proteins present in these cells, such as SK3, and this would increase as localised CAG expansion occurs with ageing.

Discussion

This study is the first to directly address the intrinsic functional membrane properties of midbrain DA neurones in mouse models of Huntington's disease. We have used tissues that

correspond to both pre-manifest and manifest disease and report a marked increase in the excitability of DA neurones that is evident at an early stage of disease progression. This results in profound alterations in dopamine release which presents as an increased evoked release in the presymptomatic condition and, in sharp contrast, near extinction in overt disease. In addition, these changes occur in the context of ongoing CAG repeat expansion, and disruption of SK3 channels expression in the DA neurones of the *SNc*.

Membrane properties

The passive membrane properties of control DA neurones were found to be comparable to those reported elsewhere [37,38,48–50]. Importantly, R6/1-89Q and R6/1 DA neurones exhibited normal membrane properties (Table 1) suggesting that they are relatively preserved from morphological and intrinsic degenerative changes. This is in marked contrast with several HD mouse studies that report changes in the passive membrane properties of striatal medium spiny neurones [51–53], hippocampal pyramidal cells and cortical neurones [28,54]. However, the tonic properties of transgenic DA cells were found to be profoundly altered. The most conspicuous alteration displayed by both R6/1 and R6/1-89Q DA neurones was a striking impairment of the slow AHP. In DA neurones the AHP is mediated by a class of small conductance calcium-activated potassium channels known as SK3 channels [43,44]. The profound loss of the AHP, and the consequent increase in neuronal excitability and reduced accommodation associated with it, strongly suggest that there is a functional lesion at the level of the SK3 channel. The alterations in the level of SK3 expression we observed in both R6/1 and R6/1-89Q line support the view that such lesion is an early event in the pathologic phenotype of DA neurones in HD.

Dopamine release

One would predict that an increase in neuronal excitability of DA cells might manifest as a functional increase in the release of dopamine from these cells, and indeed this seems to be the case for presymptomatic R6/1-89Q mice. Furthermore, it has recently been shown using microdialysis that dopamine and its metabolites are markedly increased in a conditional mouse model deficient in SK3 channels [55]. In contrast, studies in the short-lived R6/2 mouse line suggested that dopamine release is actually reduced [24,27], though one study indicated a transient increase in the activity of tyrosine hydroxylase in presymptomatic R6/2

mice [56]. Importantly, two recent studies provide indirect functional evidence that DA tone is enhanced in the striatum during early-stage disease [57,58]. In one study using R6/1 mice, the majority of striatal neurones exhibited high gamma-oscillations, a form of high frequency activation not normally seen in normal mice. Such oscillations are reported in Parkinson's disease patients undergoing dopamine supplementation and in rats treated with dopamine agonists [59,60]. Our finding that striatal dopamine release is greatly augmented in presymptomatic R6/1-89Q mice supports the view that enhanced levels of striatal dopamine is a feature of early stage disease and may underlie emergent properties such as high gamma-oscillations. Furthermore, the decrease in dopamine receptor densities reported in the striata of presymptomatic and early symptomatic human gene carriers [16–19] may also reflect a compensatory down regulation in dopamine receptor expression levels in these individuals in response to elevated levels of striatal dopamine.

The prediction that increased neuronal excitability leads to enhanced dopamine release does not hold for symptomatic animals. In sharp contrast, dopamine release was found to be severely reduced in striatal slices from R6/1 mice and is in accordance with previous investigations showing that dopamine release is also reduced [26,61]. This failure in release is likely to reflect an impairment of the release mechanism itself. Petersen and colleagues [61] demonstrated that in R6/1 mice there was a reduction of 70% in extracellular dopamine but found no change in striatal tyrosine hydroxylase immunoreactivity. Moreover, huntingtin is known to associate with microtubules and synaptic vesicles at nerve terminals [62–64] and mutant huntingtin, in a cultured PC12 cell model, impairs both the expression of the SNARE-associated protein complexin II and the release of catecholamines from dense core vesicles [65].

Our data from this comparative study suggests that the profile of dopamine release in HD may be biphasic in nature: presymptomatic and early stages of the disease being associated with elevated levels of striatal dopamine and later stages associated with a near dearth of dopamine. Consistent with this view is the observation that YAC 128 mice exhibit a period of behavioural hyperactivity prior to the development of a motor deficit and in turn is followed by hypokinesis [66]; a pattern of activity that mirrors a biphasic DA profile of release.

Mechanism

The loss of SK3 channel function appears to be an early and sustained functional deficit of DA neurones in this study. It is also worth noting that we see little indication of heterogeneity between cells or between animals, suggesting that this loss of channel function is uniform and offering a potential physiological measure with which to assess the efficacy of preventative therapeutics in preclinical testing. The mechanism underlying this loss may be attributable to an interaction between the transgenic protein and the SK3 channel protein, such that these channels are rendered non-functional or are incorrectly distributed within the DA neurones. This hypothesis is clearly supported by our immunolabelling of SK3 channels as SK3 protein distribution was found to be altered in R6/1 mice. However, colocalization between large aggregates and SK3 was not obvious, suggesting that the non-aggregated, soluble or micro-aggregate form of the transgenic protein may be the critical effector protein in the interaction. Transgenic polyglutamine proteins have been shown to exert effects upon other essential cellular components by polyglutamine-polyglutamine interactions. Several proteins containing stretches of expanded polyglutamines have been shown to be sequestered by transgenic polyglutamine-containing proteins, including TBP, CBP [67], BRN2 [68] and NF-Y [69]. In our study we have demonstrated, by analysing gDNA and mRNA, that the transgenic CAG repeat undergoes progressive expansion and is expressed throughout the lifetime of the R6/1-89Q line. Based upon the expansion profiles we observe, we would predict that the transgenic protein in the individual DA neurones of the *SNc* carry between 89 and 143 glutamine residues. SK3 channels, encoded by the *kcnn3* gene, also contain a stretch of polyglutamine residues close to the amino terminus and therefore constitute a potential target for sequestration by the polyglutamine containing transgenic protein. Our triple immunolabelling data indeed suggest that the distribution of the protein within the cell is profoundly affected and that it may be the case that the apparent increase in SK3 levels observed are due to attempts to compensate for loss of channel function. Furthermore, as CAG repeat expansion in the *SNc* was evident as early as 2 months of age in these animals, it is easy to see how a cycle of increasing sequestration could occur during the pre-phenotypic stages of this animal's life. Thus, the R6/1-89Q mouse model may provide an excellent model for further investigation of pre-manifest HD. Interestingly, polymorphisms in the CAG repeat of the *kcnn3* gene have also been implicated in cognitive performance, schizophrenia and bipolar disorder [70–73], suggesting that polyglutamine interactions are a normal aspect of SK3 channel function and/or regulation.

Based upon our observations in DA neurones, it is clear that they appear to be vulnerable to CAG repeat expansion. This vulnerability may, in itself, be a consequence, *per*

se, of dopamine. High levels of dopamine are believed to be neurotoxic and are known to promote the formation of damaging reactive oxygen species [74]. Oxygen radicals can damage DNA and it has been shown that repair of damaged DNA mediated by the OGG1 repair enzyme can lead to CAG repeat expansion [75]. The excitatory amino acid, glutamate, has also been shown to initiate DNA damage [76] and this may be further aggravated by dopamine [77]. This suggests that a cycle of DNA damage, repair and expansion may occur within this cell population, with increased damage being promoted through the physiological effects of SK3 sequestration and increased levels of dopamine release in the early stages of HD. Moreover, other cells, such as medium spiny neurones, exposed to high levels of dopamine released from DA neurones may themselves be subject to DNA damage and potential CAG expansion and consequent polyglutamine associated toxicity. Interestingly, it has been shown that an HD mouse model with raised levels of dopamine, produced by breeding with a dopamine transporter knockout mouse, developed aggregates within the striatum at an enhanced rate [32]. In the context of our experiments, an initial CAG repeat of 89Q in the mouse is sufficient to render SK3 channels dysfunctional. This observation may provide an explanation for why the drug riluzole had limited efficacy in slowing disease progression in a recent clinical trial [78]. One of the pharmacological actions of riluzole is the activation of SK3 channels [79]; it is therefore possible that failure to demonstrate efficacy in the trial may be because the SK3 channels were no longer capable of being activated. In terms of the human condition, a greater understanding of the relationship between SK3 channel sequestration and the CAG repeat length of mutant huntingtin may provide critical insight into a potential tipping point in the early pathogenesis of HD.

In conclusion, the data we provide here suggests a biphasic change in dopamine bioavailability during the progression of the disease phenotype and this reconciles a number of reports questioning the role of dopamine in HD. More importantly, our results strongly support the view that an early event in the pathogenesis of HD is a selective loss of functional SK3 channels in DA cells. These data suggest that early therapeutic interventions designed to limit the excess of dopamine, such as the dopamine depleting agent tetrabenzine, and DNA damage in presymptomatic gene carriers may be efficacious in slowing disease progression. Furthermore, our observation in R6/1-89Q mice that changes in the evoked cell properties of mid-brain DA neurones are uniform, suggests that such presymptomatic cellular phenotypes could form the basis as a means to assess the efficacy of early treatments in pre-clinical screening programmes.

Acknowledgments

This work was supported by the Open University Research Development Fund and the Royal Society. We would like to thank Professor Gillian Bates FRS for the kind gift of the S830 antibody.

References

1. Paulsen JS, Ready RE, Hamilton JM, Mega MS, Cummings JL: Neuropsychiatric aspects of Huntington's disease. J Neurol Neurosurg Psychiatry 2001 Sep 1;71:310–4.

2. Becher MW, Kotzuk J a, Sharp AH, Davies SW, Bates GP, Price DL, et al.: Intranuclear neuronal inclusions in Huntington's disease and dentatorubral and pallidoluysian atrophy: correlation between the density of inclusions and IT15 CAG triplet repeat length. Neurobiol Dis 1998 Apr;4:387–397.

3. Harper P: Huntington's Disease; in Saunders WB (ed): Major Problems of Neurology. 2nd ed. Philadelphia, Pa: WB Saunders; 1996. PA, USA, 1996.

4. Foldstein S.: Huntington's Disease. Baltimore, USA, 1990.

5. Hedreen JC, Peyser CE, Folstein SE, Ross CA: Neuronal loss in layers V and VI of cerebral cortex in Huntington's disease. Neurosci Lett 1991 Dec 9 [cited 2011 Oct 13];133:257–61.

6. Utal a: PEP-19 immunohistochemistry defines the basal ganglia and associated structures in the adult human brain, and is dramatically reduced in Huntington's disease. Neuroscience 1998 Jun 18;86:1055–1063.

7. Vonsattel JP, Myers RH, Stevens TJ, Ferrante RJ, Bird ED, Richardson Jr. EP: Neuropathological classification of Huntington's disease. J Neuropathol Exp Neurol 1985;44:559–577.

8. Foroud T, Siemers E, Kleindorfer D, Bill DJ, Hodes ME, Norton JA, et al.: Cognitive scores in carriers of Huntington's disease gene compared to noncarriers. Ann Neurol 1995;37:657–664.

9. Lange KW, Sahakian BJ, Quinn NP, Marsden CD, Robbins TW: Comparison of executive and visuospatial memory function in Huntington's disease and dementia of Alzheimer type matched for degree of dementia. J Neurol Neurosurg Psychiatry 1995;58:598–606.

10. Lawrence a. D, Weeks RA, Brooks DJ, Andrews TC, Watkins LH, Harding AE, et al.: Evidence for specific cognitive deficits in preclinical Huntington's disease. Brain 1998 Jul 1;121 Pt 7:1329–1341.

11. Lawrence AD, Sahakian BJ, Hodges JR, Rosser AE, Lange KW, Robbins TW: Executive and mnemonic functions in early Huntington's disease. Brain 1996;119. Pt 5:1633–1645.

12. Mohr E, Brouwers P, Claus JJ, Mann UM, Fedio P, Chase TN: Visuospatial cognition in Huntington's disease. Mov Disord 1991;6:127–132.

13. Snowden JS, Craufurd D, Thompson J, Neary D: Psychomotor, executive, and memory function in preclinical Huntington's disease. J Clin Exp Neuropsychol 2002 Apr;24:133–145.

14. Lemiere J, Decruyenaere M, Evers-Kiebooms G, Vandenbussche E, Dom R: Cognitive changes in patients with Huntington's disease (HD) and asymptomatic carriers of the HD mutation--a longitudinal follow-up study. J Neurol 2004;251:935–942.

15. Berrios GE, Wagle a. C, Markova IS, Wagle S a., Rosser a., Hodges JR: Psychiatric symptoms in neurologically asymptomatic Huntington's disease gene carriers: a comparison with gene negative at risk subjects. Acta Psychiatr Scand 2002 Mar;105:224–230.

16. Andrews TC, Weeks RA, Turjanski N, Gunn RN, Watkins LH, Sahakian B, et al.: Huntington's disease progression: PET and clinical observations. Brain 1999 Dec 1;122:2353–2363.

17. Pavese N, Andrews TC, Brooks DJ, Ho AK, Rosser AE, Barker RA, et al.: Progressive striatal and cortical dopamine receptor dysfunction in Huntington's disease: a PET study. Brain 2003 May 1;126:1127–1135.

18. Ginovart N, Lundin A, Farde L, Halldin C, Bäckman L, Swahn CG, et al.: PET study of the pre- and post-synaptic dopaminergic markers for the neurodegenerative process in Huntington's disease. Brain 1997 Mar 1;120:503–514.

19. Van Oostrom JC, Maguire RP, Verschuuren-Bemelmans CC, Veenma-van der Duin L, Pruim J, Roos RA, et al.: Striatal dopamine D2 receptors, metabolism, and volume in preclinical Huntington disease . Neurology 2005;65:941–943.

20. André VM, Cepeda C, Levine MS: Dopamine and glutamate in Huntington's disease: A balancing act. CNS Neurosci Ther 2010 Jun;16:163–78.

21. Miller BR, Bezprozvanny I: Corticostriatal circuit dysfunction in Huntington's disease: intersection of glutamate, dopamine and calcium. Future Neurol 2010 Sep;5:735–756.

22. Huntington's Disease Collaborative Research Group: A novel gene containing a trinucleotide repeat that is expanded and unstable on Huntington's disease chromosomes. Cell 1993;72:971–983.

23. Bates G, Murphy KPSJ: Mouse models of Huntington's disease; in : Huntington's Disease. 2002.

24. Johnson M a, Rajan V, Miller CE, Wightman RM: Dopamine release is severely compromised in the R6/2 mouse model of Huntington's disease. J Neurochem 2006 May;97:737–746.

25. Bibb JA, Yan Z, Svenningsson P, Snyder GL, Pieribone V a, Horiuchi A, et al.: Severe deficiencies in dopamine signaling in presymptomatic Huntington's disease mice. Proc Natl Acad Sci U S A 2000 Jun 6;97:6809–6814.

26. Ortiz AN, Kurth BJ, Osterhaus GL, Johnson M a: Impaired dopamine release and uptake in R6/1 Huntington's disease model mice. Neurosci Lett 2011 Mar 29;492:11–4.

27. Callahan JW, Abercrombie ED: In vivo Dopamine Efflux is Decreased in Striatum of both Fragment (R6/2) and Full-Length (YAC128) Transgenic Mouse Models of Huntington's Disease. Front Syst Neurosci 2011 Jan;5:61.

28. Cummings DM, Milnerwood AJ, Dallérac GM, Waights V, Brown JY, Vatsavayai SC, et al.: Aberrant cortical synaptic plasticity and dopaminergic dysfunction in a mouse model of Huntington's disease. Hum Mol Genet 2006 Oct 1;15:2856–68.

29. Dallérac GM, Vatsavayai SC, Cummings DM, Milnerwood AJ, Peddie CJ, Evans KA, et al.: Impaired Long-Term Potentiation in the Prefrontal Cortex of Huntington's Disease Mouse Models: Rescue by D(1) Dopamine Receptor Activation. Neurodegener Dis 2011;8:230–9.

30. Jahanshahi A, Vlamings R, Kaya AH, Lim LW, Janssen MLF, Tan S, et al.: Hyperdopaminergic status in experimental Huntington disease. J Neuropathol Exp Neurol 2010 Sep;69:910–7.

31. Charvin D, Roze E, Perrin V, Deyts C, Betuing S, Pagès C, et al.: Haloperidol protects striatal neurons from dysfunction induced by mutated huntingtin in vivo. Neurobiol Dis 2008 Jan;29:22–9.

32. Cyr M, Sotnikova TD, Gainetdinov RR, Caron MG: Dopamine enhances motor and neuropathological consequences of polyglutamine expanded huntingtin. FASEB J 2006 Dec;20:2541–3.

33. Vatsavayai SC, Dall GM, Milnerwood AJ, Cummings DM, Rezaie P, Murphy KPSJ, et al.: Progressive CAG expansion in the brain of a novel R6 / 1-89Q mouse model of Huntington ' s disease with delayed phenotypic onset. Brain Res Bull 2007;72:98–102.

34. Van Dellen a, Blakemore C, Deacon R, York D, Hannan a J: Delaying the onset of Huntington's in mice. Nature 2000 Apr 13;404:721–722.

35. Rall W: Membrane time constant of motoneurons. Science 1957 Sep 6;126:454.

36. Grace AA, Bunney BS: Intracellular and extracellular electrophysiology of nigral dopaminergic neurons--1. Identification and characterization. Neuroscience 1983;10:301–315.

37. Grace AA, Onn SP: Morphology and electrophysiological properties of immunocytochemically identified rat dopamine neurons recorded in vitro. J Neurosci 1989 Oct;9:3463–3481.

38. Yung WH, Häusser M a, Jack JJ, Hausser MA: Electrophysiology of dopaminergic and non-dopaminergic neurones of the guinea-pig substantia nigra pars compacta in vitro. J Physiol 1991 May;436:643–667.

39. Phillips PEM, Hancock PJ, Stamford J a: Time window of autoreceptor-mediated inhibition of limbic and striatal dopamine release. Synapse 2002 Apr;44:15–22.

40. Grace AA, Bunney BS: The control of firing pattern in nigral dopamine neurons: single spike firing. J Neurosci 1984;4:2866–2876.

41. Gonon FG: Nonlinear relationship between impulse flow and dopamine released by rat midbrain dopaminergic neurons as studied by in vivo electrochemistry. Neuroscience 1988;24:19–28.

42. Cepeda C, Murphy KPS, Parent M, Levine MS: The role of dopamine in Huntington's disease. Prog Brain Res 2014 Jan;211:235–54.

43. Ping HX, Shepard PD: Apamin-sensitive Ca(2+)-activated K+ channels regulate pacemaker activity in nigral dopamine neurons . Neuroreport 1996;7:809–814.

44. Wolfart J, Roeper J: Selective coupling of T-type calcium channels to SK potassium channels prevents intrinsic bursting in dopaminergic midbrain neurons. J Neurosci 2002 May 1;22:3404–13.

45. Kennedy L, Shelbourne PF: Dramatic mutation instability in HD mouse striatum: does polyglutamine load contribute to cell-specific vulnerability in Huntington's disease? Hum Mol Genet 2000 Oct 1;9:2539–2544.

46. Kennedy L, Evans E, Chen CM, Craven L, Detloff PJ, Ennis M, et al.: Dramatic tissue-specific mutation length increases are an early molecular event in Huntington disease pathogenesis. Hum Mol Genet 2003;12:3359–3367.

47. Shelbourne PF, Keller-McGandy C, Bi WL, Yoon S-R, Dubeau L, Veitch NJ, et al.: Triplet repeat mutation length gains correlate with cell-type specific vulnerability in Huntington disease brain. Hum Mol Genet 2007 May 15;16:1133–42.

48. Murphy KP, Greenfield SA: Neuronal selectivity of ATP-sensitive potassium channels in guinea-pig substantia nigra revealed by responses to anoxia. J Physiol 1992;453:167–183.

49. Hajos M, Greenfield SA: Topographic heterogeneity of substantia nigra neurons: diversity in intrinsic membrane properties and synaptic inputs. Neuroscience 1993;55:919–934.

50. Mercuri NB, Bonci A, Calabresi P, Stefani A, Bernardi G: Properties of the hyperpolarization-activated cation current Ih in rat midbrain dopaminergic neurons. Eur J Neurosci 1995;7:462–469.

51. Levine MS, Klapstein GJ, Koppel A, Gruen E, Cepeda C, Vargas ME, et al.: Enhanced sensitivity to N-methyl-D-aspartate receptor activation in transgenic and knock in mouse models of Huntington's disease. J Neurosci Res 1999 Nov 15;58:515–532.

52. Ariano MA, Cepeda C, Calvert CR, Flores-Hernandez J, Hernandez-Echeagaray E, Klapstein GJ, et al.: Striatal potassium channel dysfunction in Huntington's disease transgenic mice. J Neurophysiol 2005 May;93:2565–2574.

53. Klapstein GJ, Fisher RS, Zanjani H, Cepeda C, Jokel EVES, Gloria J, et al.: Electrophysiological and Morphological Changes in Striatal Spiny Neurons in R6 / 2 Huntington ' s Disease Transgenic Mice. J Neurophysiol 2001;1–3.

54. Milnerwood AJ, Cummings DM, Dallerac GM, Brown JY, Vatsavayai SC, Hirst MC, et al.: Early development of aberrant synaptic plasticity in a mouse model of Huntington's disease. Hum Mol Genet 2006 May 15;15:1690–1703.

55. Jacobsen JPR, Weikop P, Hansen HH, Mikkelsen JD, Redrobe JP, Holst D, et al.: SK3 K+ channel-deficient mice have enhanced dopamine and serotonin release and altered emotional behaviors. Genes Brain Behav 2008 Nov;7:836–48.

56. Yohrling GJ th, Jiang GC, DeJohn MM, Miller DW, Young AB, Vrana KE, et al.: Analysis of cellular, transgenic and human models of Huntington's disease reveals tyrosine hydroxylase alterations and substantia nigra neuropathology. Brain Res Mol Brain Res 2003 Nov 6;119:28–36.

57. Cayzac S, Delcasso S, Paz V, Jeantet Y, Cho YH: Changes in striatal procedural memory coding correlate with learning deficits in a mouse model of Huntington disease. Proc Natl Acad Sci U S A 2011 May 31;108:9280–5.

58. André VM, Cepeda C, Fisher YE, Huynh M, Bardakjian N, Singh S, et al.: Differential electrophysiological changes in striatal output neurons in Huntington's disease. J Neurosci 2011 Jan 26;31:1170–82.

59. Berke JD: Fast oscillations in cortical-striatal networks switch frequency following rewarding events and stimulant drugs. Eur J Neurosci 2009 Sep;30:848–59.

60. Burkhardt JM, Jin X, Costa RM: Dissociable effects of dopamine on neuronal firing rate and synchrony in the dorsal striatum. Front Integr Neurosci 2009 Jan;3:28.

61. Petersén Å, Puschban Z, Lotharius J, NicNiocaill B, Wiekop P, O'Connor WTT, et al.: Evidence for dysfunction of the nigrostriatal pathway in the R6/1 line of transgenic Huntington's disease mice. Neurobiol Dis 2002 Oct;11:134–146.

62. DiFiglia M, Sapp E, Chase K, Schwarz C, Meloni A, Young C, et al.: Huntingtin is a cytoplasmic protein associated with vesicles in human and rat brain neurons. Neuron 1995 May;14:1075–1081.

63. Gutekunst C a, Levey AI, Heilman CJ, Whaley WL, Yi H, Nash NR, et al.: Identification and localization of huntingtin in brain and human lymphoblastoid cell lines with anti-fusion protein antibodies. Proc Natl Acad Sci U S A 1995 Sep 12;92:8710–8714.

64. Sharp AH, Loev SJ, Schilling G, Li SH, Li XJ, Bao J, et al.: Widespread expression of Huntington's disease gene (IT15) protein product. Neuron 1995;14:1065–1074.

65. Edwardson JM, Wang C-TT, Gong B, Wyttenbach A, Bai J, Jackson MB, et al.: Expression of mutant huntingtin blocks exocytosis in PC12 cells by depletion of complexin II. J Biol Chem 2003 Aug 15;278:30849–30853.

66. Slow EJ, van Raamsdonk J, Rogers D, Coleman SH, Graham RK, Deng Y, et al.: Selective striatal neuronal loss in a YAC128 mouse model of Huntington disease. Hum Mol Genet 2003 Jul 1;12:1555–1567.

67. Schaffar G, Breuer P, Boteva R, Behrends C, Tzvetkov N, Strippel N, et al.: Cellular toxicity of polyglutamine expansion proteins: mechanism of transcription factor deactivation. Mol Cell 2004 Jul 2;15:95–105.

68. Yamanaka T, Tosaki A, Miyazaki H, Kurosawa M, Furukawa Y, Yamada M, et al.: Mutant huntingtin fragment selectively suppresses Brn-2 POU domain transcription factor to mediate hypothalamic cell dysfunction. Hum Mol Genet 2010 Jun 1;19:2099–112.

69. Yamanaka T, Miyazaki H, Oyama F, Kurosawa M, Washizu C, Doi H, et al.: Mutant Huntingtin reduces HSP70 expression through the sequestration of NF-Y transcription factor. EMBO J 2008 Mar 19;27:827–39.

70. Gargus JJ, Fantino E, Gutman G a: A piece in the puzzle: an ion channel candidate gene for schizophrenia. Mol Med Today 1998 Dec;4:518–24.

71. Chandy KG, Fantino E, Wittekindt O, Kalman K, Tong LL, Ho TH, et al.: Isolation of a novel potassium channel gene hSKCa3 containing a polymorphic CAG repeat: a candidate for schizophrenia and bipolar disorder? Mol Psychiatry 1998 Jan [cited 2011 Oct 8];3:32–7.

72. Ritsner M, Modai I, Ziv H, Amir S, Halperin T, Weizman A, et al.: An association of CAG repeats at the KCNN3 locus with symptom dimensions of schizophrenia.Biol Psychiatry 2002 May 15;51:788–94.

73. Dror V, Shamir E, Ghanshani S, Kimhi R, Swartz M, Barak Y, et al.: hKCa3/KCNN3 potassium channel gene: association of longer CAG repeats with schizophrenia in Israeli Ashkenazi Jews, expression in human tissues and localization to chromosome 1q21. Mol Psychiatry 1999 May; 4:254–60.

74. Chen L, Ding Y, Cagniard B, Van Laar AD, Mortimer A, Chi W, et al.: Unregulated cytosolic dopamine causes neurodegeneration associated with oxidative stress in mice. J Neurosci 2008 Jan 9;28:425–33.

75. Kovtun I V, Liu Y, Bjoras M, Klungland A, Wilson SH, McMurray CT: OGG1 initiates age-dependent CAG trinucleotide expansion in somatic cells. Nature 2007 May 24;447:447–52.

76. Yang J-L, Tadokoro T, Keijzers G, Mattson MP, Bohr VA: Neurons efficiently repair glutamate-induced oxidative DNA damage by a process involving CREB-mediated up-regulation of apurinic endonuclease 1. J Biol Chem 2010 Sep 3;285:28191–9.

77. Paoletti P, Vila I, Rifé M, Lizcano JM, Alberch J, Ginés S: Dopaminergic and glutamatergic signaling crosstalk in Huntington's disease neurodegeneration: the role of p25/cyclin-dependent kinase 5. J Neurosci 2008 Oct 1;28:10090–101.

78. Landwehrmeyer GB, Dubois B, de Yébenes JG, Kremer B, Gaus W, Kraus PH, et al.: Riluzole in Huntington's disease: a 3-year, randomized controlled study. Ann Neurol 2007 Sep;62:262–72.

79. Liu B-S, Ferreira R, Lively S, Schlichter LC: Microglial SK3 and SK4 currents and activation state are modulated by the neuroprotective drug, riluzole. J Neuroimmune Pharmacol 2013 Mar;8:227–37.

Tables

Cell property	Control	R6/1-89Q	R6/1	p
E_0 (mV)	-57.6 ± 1.50	-55.09 ± 2.60	-55.58 ± 0.77	0.22
Ri (MΩ)	108.76 ± 5.02	102.94 ± 5.99	122.45 ± 10.20	0.93
T_0 (ms)	21.91 ± 1.52	23.23 ± 3.55	16.87 ± 2.47	0.13
T_1 (ms)	1.66 ± 0.08	1.66 0.10	1.61 ± 0.11	0.24
L	0.92 ± 0.04	0.9 ± 0.05	1.06 ± 0.07	0.19
C (nF)	0.23 ± 0.02	0.24 ± 0.04	0.16 ± 0.03	0.16

Table 1

AP property	Control	R6/1-89Q	R6/1
Threshold (mV)	-37.50 ± 1.12	-40.06 ± 1.22	-37.69 ± 2.61
Amplitude (mV)	56.69 ± 1.63	48.1 ± 1.42*	51.06 ± 2.02**
Overshoot (mV)	19.25 ± 1.48	11.25 ± 2.46**	11.04 ± 2.04*
Width (ms)	0.97 ± 0.04	0.84 ± 0.05	0.83 ± 0.13
sAHP amplitude (mV)	10.35 ± 0.66	7.65 ± 1.02	3.49 ± 1.44***
sAHP duration (ms)	133.27 ± 5.95	74.68 ± 7.45***	40.73 ± 10.52***
fAHP amplitude (mV)	2.14 ± 0.36	2.81 ± 0.45	5.57 ± 1.08***
fAHP duration (ms)	15.92 ± 2.05	19.75 ± 2.19	21.09 ± 2.75

Table 2

Table and figure legends

Table 1. Passive membrane properties of transgenic dopaminergic (DA) neurones. One way ANOVA revealed no significant difference in the membrane properties of non-transgenic and transgenic DA neurones. Cm: capacitance, E_0: resting membrane potential, L: electronic length, Ri: input resistance, T_0: membrane time constant, T_1: equalizing time constant.

Table 2. AP properties of transgenic DA neurones. One way ANOVA revealed that among the different AP characteristics, the AHP and AP size were selectively impaired in the transgenic DA neurones. *p<0.05, **p<0.01, ***p<0.001.

Figure 1. Electrophysiological characteristics of DA neurones A: The slow firing pattern of DA neurones is mainly regulated by the depolarising slow oscillatory potential (SOP) and the afterhyperpolarisation (AHP). Scale bars: 200 ms, 20 mV. B: The AHP of DA neurones comprises a fast (fAHP) and slow (sAHP) component. Scale bars: 50ms, 20 mV. C: DA neurones display a prominent inward rectification upon injection of hyperpolarising current and a delayed repolarisation following cessation of the pulse. Scale bars: 100 ms, 20 mV, 2 nA. D: DA neurone AP on a protracted time scale. Note the typical hump on the downslope. Scale bars: 2 ms, 20 mV. AP: Action Potential. E: Left- The input current /voltage relationship (I/V) was used to infer the resting membrane potential of DA neurones (E_0). Right- The input resistance was calculated from the slope of the input current *vs* maximal voltage deflection (ΔEm) regression line. F: The membrane time constant (T_0) was calculated by plotting the natural log of the response expressed as percentage of the peak negative potential (%ΔEmax) to "peel" the first order exponential for timepoints lying between 5 and 15 ms. T_0 could then be read as the slope negative inverse of the regression line. The second order exponential for timepoints earlier than 5 ms was peeled by plotting the difference between the T_0 regression line from the points lying above this line and normalizing the y-intercept of the T_1 regression line to 100%. T_1 could then be read as the slope negative inverse of the normalized T_1 regression line.

Figure 2. Tonic activity of transgenic DA neurones is impaired. A: Responses to hyperpolarising pulses were similar between transgenic and non-transgenic DA neurones. B: Spontaneous firing in non-transgenic and transgenic DA neurone; note the reduced AHP in the R6/1-89Q and R6/1 lines. Scale bars: 100 ms, 10 mV. B: Distributions of the transgenic

DA neuronal firing frequencies broader than that seen in the non-transgenic littermate population. C: Amplitude and duration of the sAHP and the AP size were found significantly reduced in both transgenic lines. *p<0.05, ***p<0.001, daggers and asterisks relate to statistics comparing non-transgenic *vs* R6/1-89Q and R6/1, respectively.

Figure 3. Transgenic DA neurones are hyper-excitable. A: Typical firing of non-transgenic, R6/1-89Q and R6/1 DA neurones upon 0.6nA depolarising constant current pulses. Scale bars: 100 ms, 10 mV, 2nA. B: Instantaneous frequency (IF) was calculated by extrapolating the neuronal firing frequency if the first inter-spike interval was constant. IF increased linearly with the current intensity for all genotypes (left) and was significantly higher in both R6/1-89Q and R6/1 lines (right). C: Total frequency corresponds to the total number of spikes normalized to one second. TF increased in a dose-response manner (left) and was significantly higher in both R6/1 lines compared to non-transgenic controls (right). C: The maximum level of accommodation occurred between the second and the first inter-spike interval (I2/I1) and increased with current intensity. The average level of accommodation between I2 and I1 for all current intensities was found to be significantly lower in both transgenic lines (right). I(n): Interval (n). *p<0.05, **p<0.01, ***p<0.001, daggers and stars relate to statistics comparing non-transgenic *vs* R6/1-89Q and R6/1, respectively.

Figure 4. Dopamine release is altered in R6/1 and R6/1-89Q transgenic mice. A: Calibration curve of the current reading as a function of dopamine concentration followed a linear relationship and is presented here on a logarithmic time scale. B: Single pulses were sufficient to generate a faradaic response of which the amplitude was used as an index of the amount of dopamine released. C: Input/output relationships revealed that significantly more dopamine was released in the R6/1-89Q while on the contrary liberation of dopamine was drastically reduced in the R6/1 mice. DAmax representative traces are shown. Scale bars: 20 pA, 500 ms. D: Paired pulse inhibition was found to be normal in the R6/1-89Q mice and impaired in the R6/1 line. *p<0.05, **p<0.01, ***p<0.001, daggers and asterisks relate to statistics comparing non-transgenic *vs* R6/1-89Q and R6/1, respectively.

Figure 5: SK3 protein expression in R6/1 transgenic mice. A: Photomicrographs of DA cells (x40) showing the increase in SK3 expression and the altered distribution of the protein in R6/1 animals. B: Analysis of the cellular SK3 fluorescence intensity (Alexa 488) revealed a

significant increase in SK3 signal in R6/1 mice. C: Such increase was not observed in non-DA (TH-negative) cells. D: Cytoplasm (C) *vs* nucleus (N) fluorescence intensity analysis shows that the intracellular distribution of the SK3 protein is perturbed. E: S830-positive cells showed a significantly higher level of SK3 fluorescence intensity, suggesting that the mutant protein segregate SK3 channels.

Figure 6: SK3 protein expression in R6/1-89Q transgenic mice. A-B: Photomicrographs of DA cells (x40) showing the increase in SK3 expression in 10 (A) and 20 (B) months old R6/1-89Q mice. C: SK3 mean fluorescence analysis revealed that the protein expression increases at both pre-manifest and manifest disease stages.

Figure 7: Cellular events in the *SNc* of R6/1-89Q mice. A: genomic DNA repeat expansion in the *SNc* occurs as early as 2 months of age in the R6/1-89Q *SNc* and is markedly aggravated at 12 months of age. B: mRNA repeat instability analysis mirror the expansion profile observed in nigral gDNA at 2 and 12MO in the R6/1-89Q.

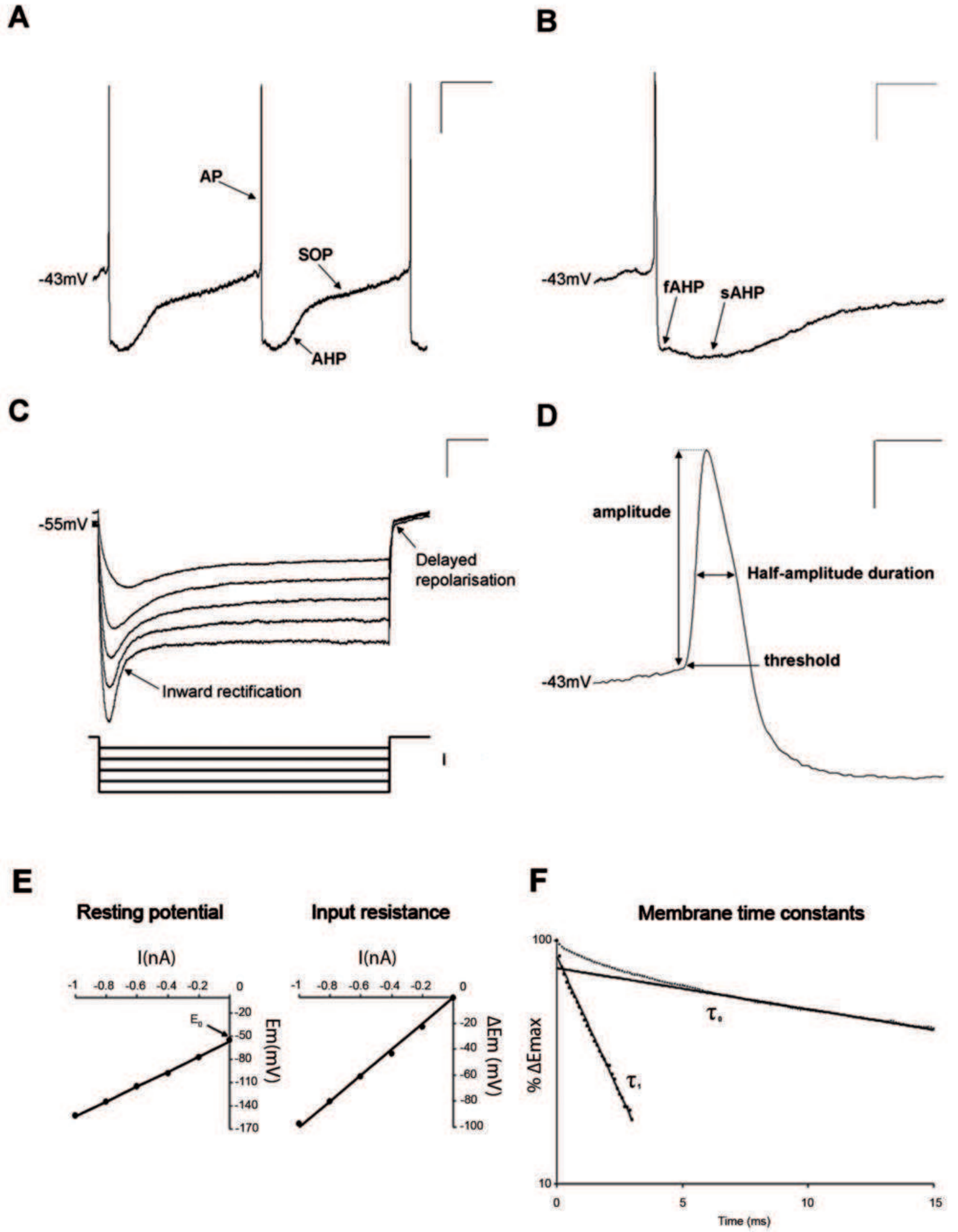
A
AP
SOP
AHP
-43mV
B
fAHP
sAHP
-43mV
C
-55mV
Delayed repolarisation
Inward rectification
I
D
amplitude
Half-amplitude duration
threshold
-43mV
E
Resting potential
I(nA)
-1 -0.8 -0.6 -0.4 -0.2 0
-20 -50 -80 -110 -140 -170
Em(mV)
Input resistance
I(nA)
-1 -0.8 -0.6 -0.4 -0.2 0
-20 -40 -60 -80 -100
ΔEm (mV)
F
Membrane time constants
100
10
% ΔEmax
τ0
τ1
0 5 10 15
Time (ms)

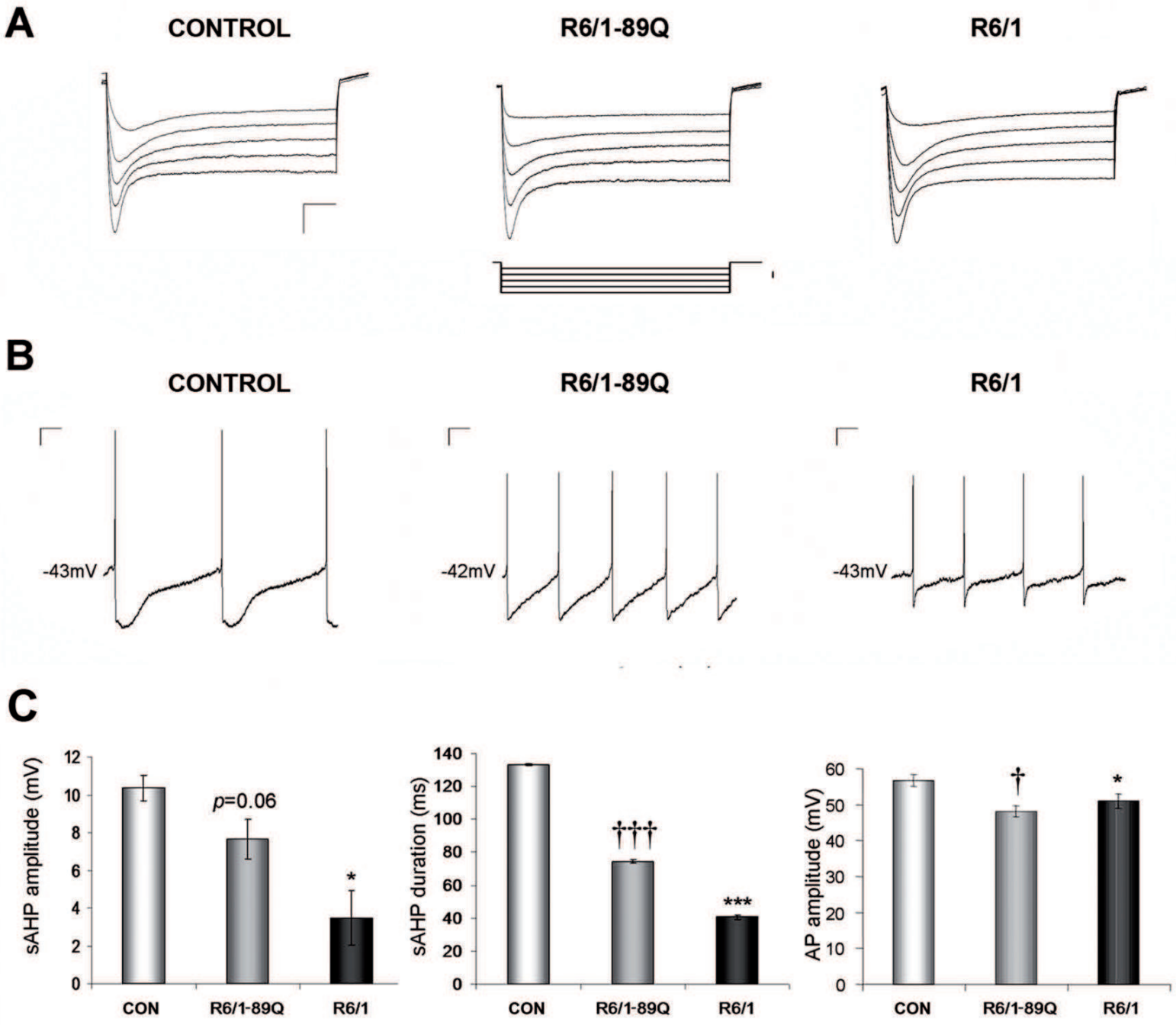
A
CONTROL
R6/1-89Q
R6/1
B
CONTROL
R6/1-89Q
R6/1
-43mV
-42mV
-43mV
C
sAHP amplitude (mV)
p=0.06
*
CON
R6/1-89Q
R6/1
sAHP duration (ms)
†††
***
CON
R6/1-89Q
R6/1
AP amplitude (mV)
†
*
CON
R6/1-89Q
R6/1

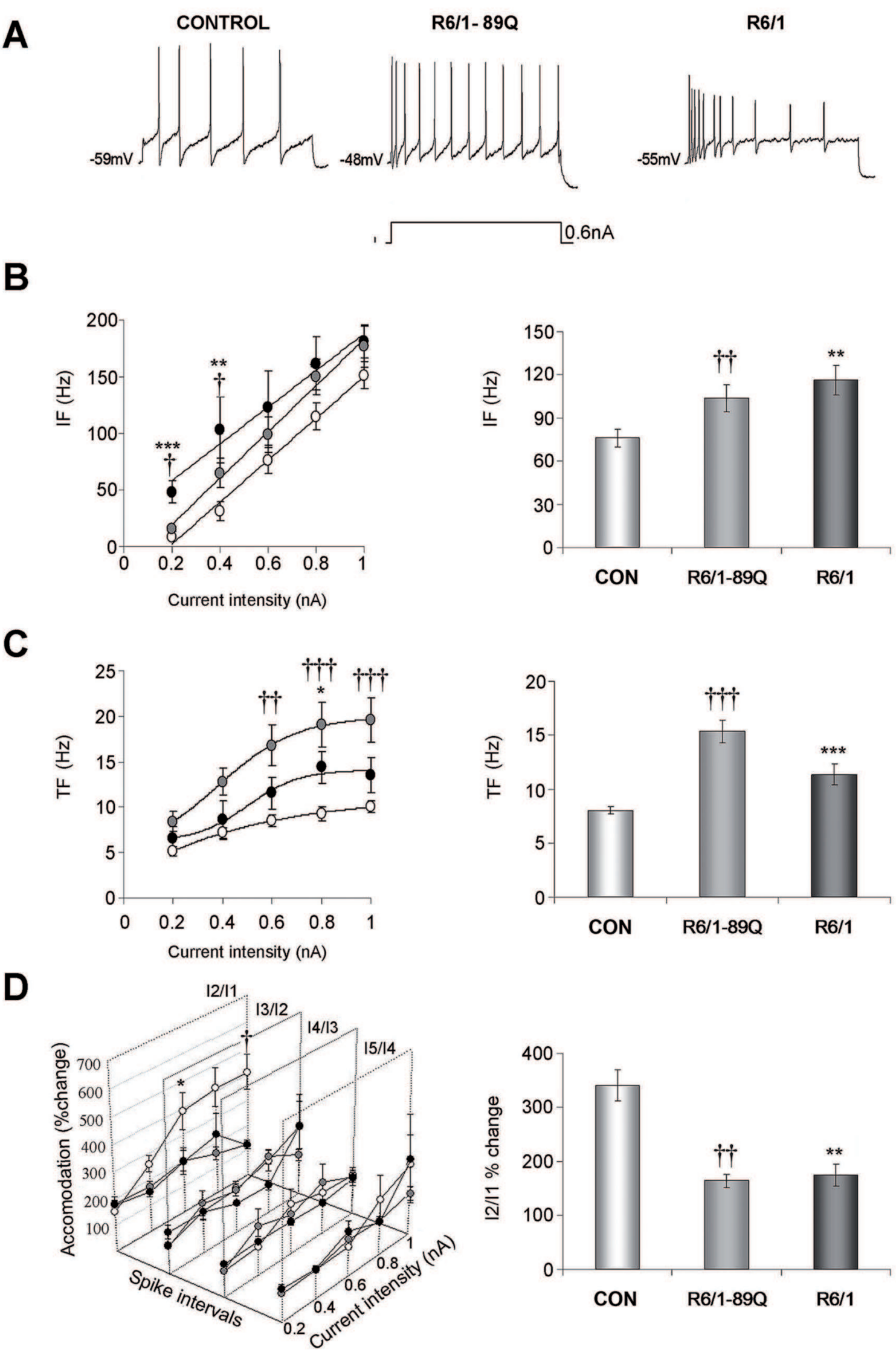
A
CONTROL
R6/1- 89Q
R6/1
-59mV
-48mV
-55mV
0.6nA
B
IF (Hz)
Current intensity (nA)
CON
R6/1-89Q
R6/1
C
TF (Hz)
Current intensity (nA)
CON
R6/1-89Q
R6/1
D
I2/I1
I3/I2
I4/I3
I5/I4
Accomodation (%change)
Spike intervals
Current intensity (nA)
I2/I1 % change
CON
R6/1-89Q
R6/1

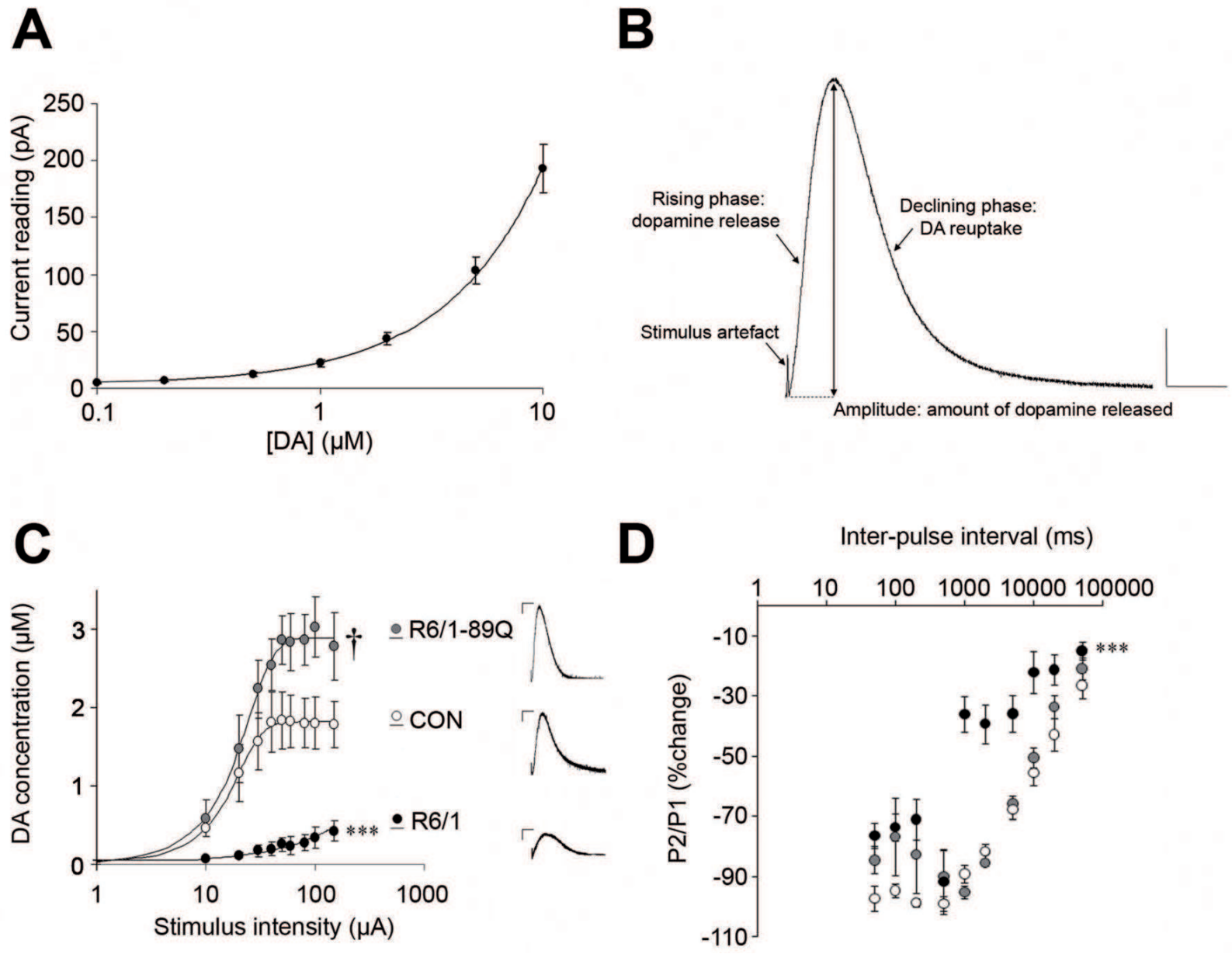
A
Current reading (pA)
250
200
150
100
50
0
0.1
1
10
[DA] (μM)
B
Rising phase:
dopamine release
Declining phase:
DA reuptake
Stimulus artefact
Amplitude: amount of dopamine released
C
DA concentration (μM)
3
2
1
0
1
10
100
1000
Stimulus intensity (μA)
R6/1-89Q
CON
R6/1
†
***
D
Inter-pulse interval (ms)
1
10
100
1000
10000
100000
P2/P1 (%change)
-10
-30
-50
-70
-90
-110
***

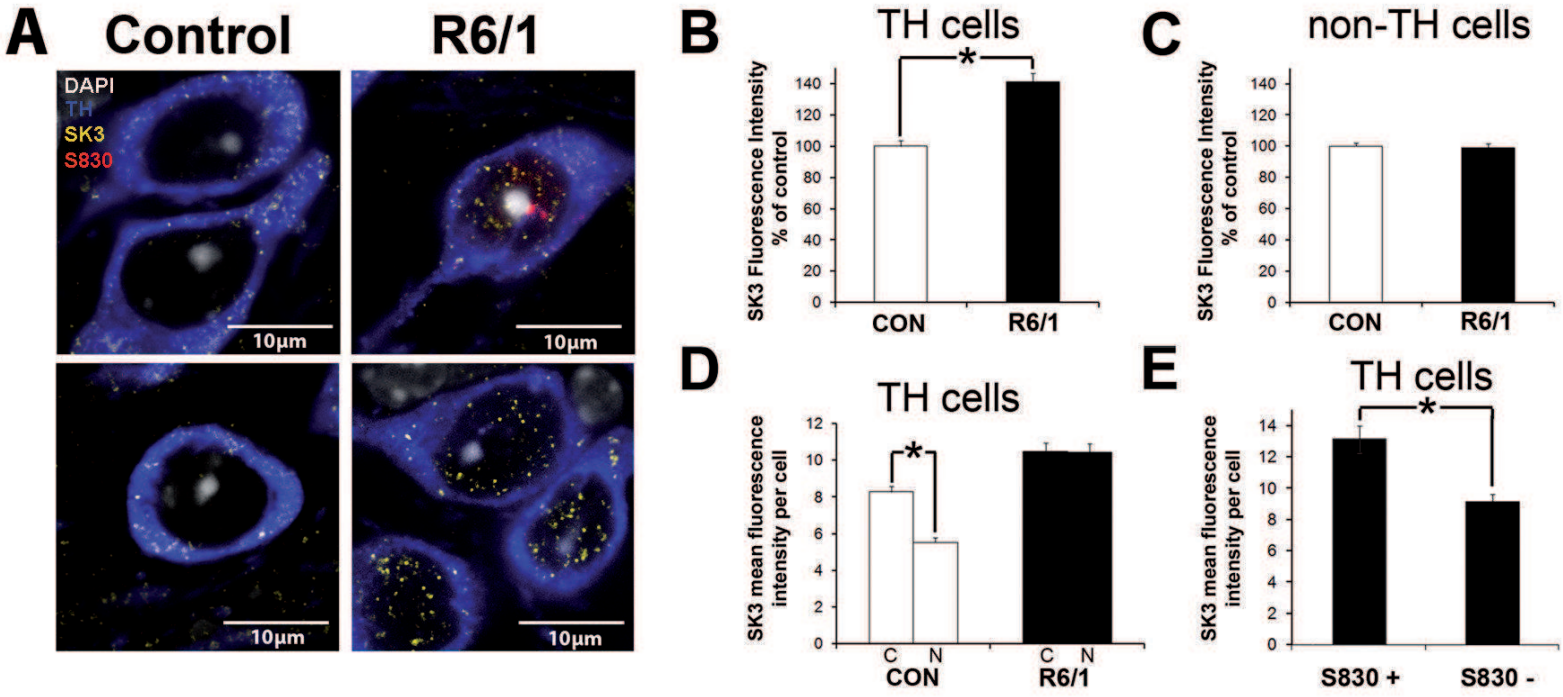
A
Control
R6/1
DAPI
TH
SK3
S830
10µm
10µm
10µm
10µm
B
TH cells
SK3 Fluorescence Intensity
% of control
CON
R6/1
C
non-TH cells
SK3 Fluorescence Intensity
% of control
CON
R6/1
D
TH cells
SK3 mean fluorescence
intensity per cell
C N
CON
C N
R6/1
E
TH cells
SK3 mean fluorescence
intensity per cell
S830 +
S830 -

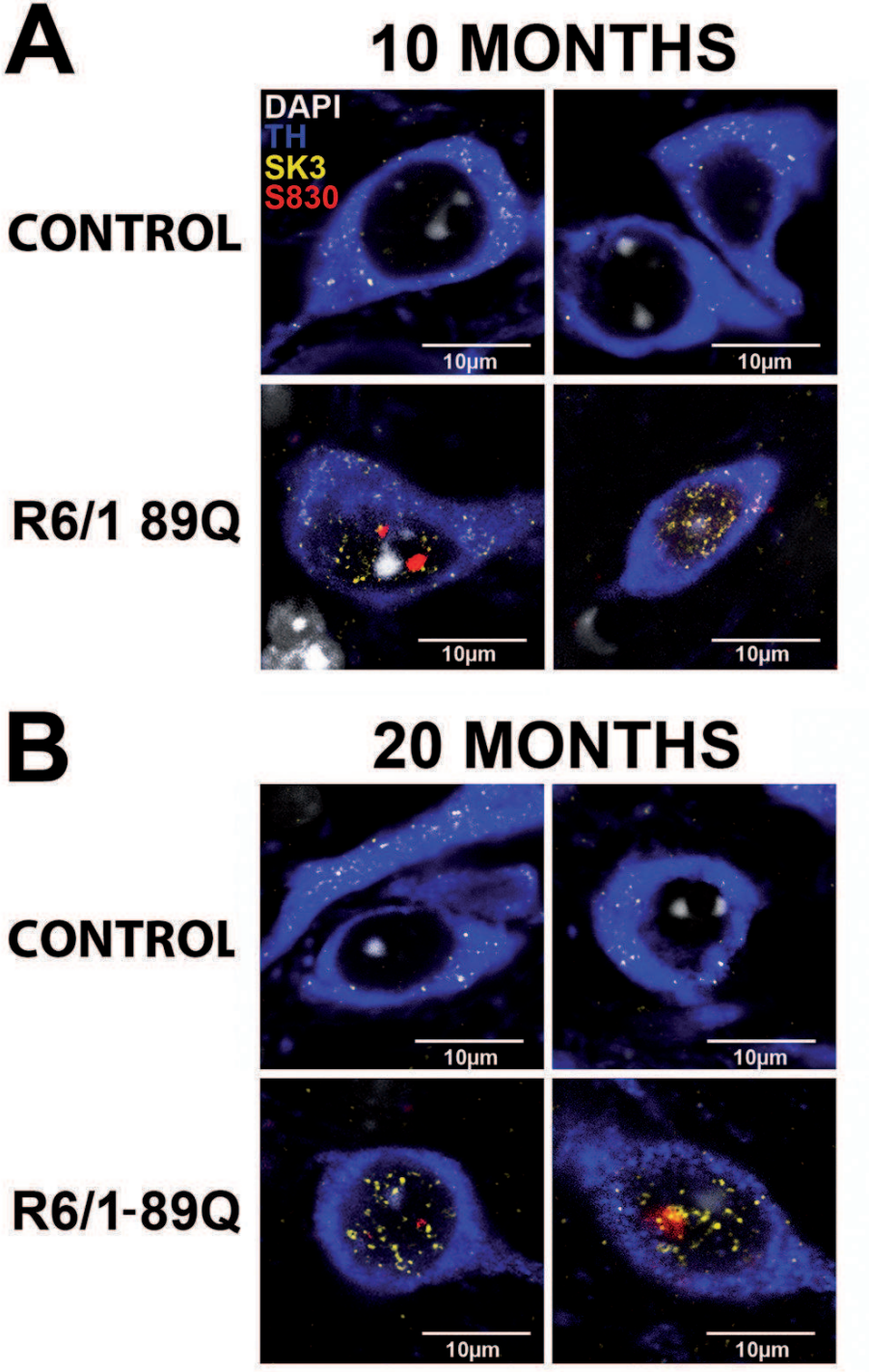
A
10 MONTHS
DAPI
TH
SK3
S830
CONTROL
R6/1 89Q
10µm
B
20 MONTHS
CONTROL
R6/1-89Q
10µm
C
SK3 fluorescence intensity
% of control
160
140
120
100
80
60
40
20
0
*
*
CON
10MO
R6/1-89Q
10MO
CON
20MO
R6/1-89Q
20MO

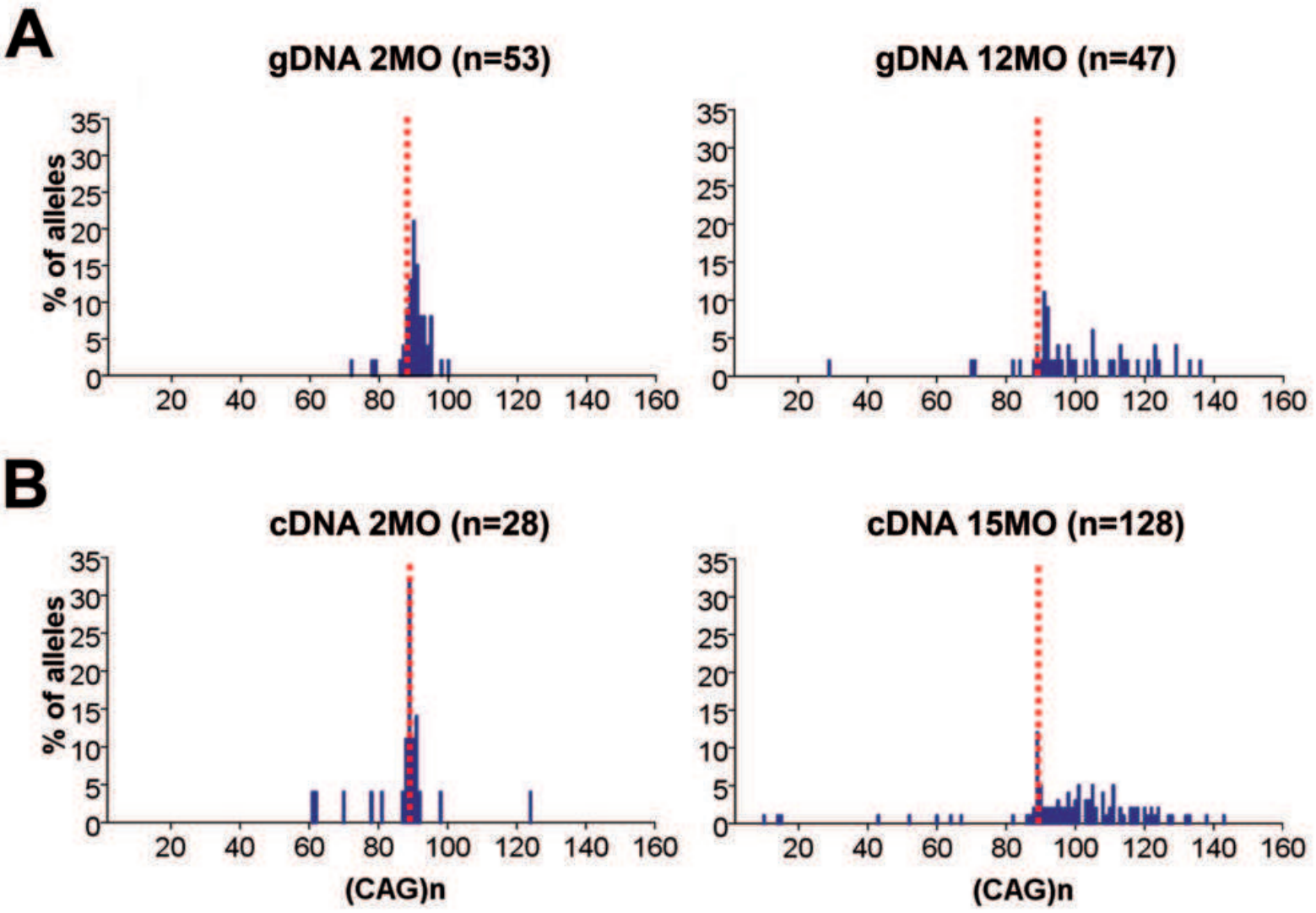
A
gDNA 2MO (n=53)
gDNA 12MO (n=47)
% of alleles
0
5
10
15
20
25
30
35
20
40
60
80
100
120
140
160
B
cDNA 2MO (n=28)
cDNA 15MO (n=128)
% of alleles
(CAG)n
(CAG)n